Constrained reconstructions for 4D intervention guidance

2013 Phys. Med. Biol. 58 3283

(http://iopscience.iop.org/0031-9155/58/10/3283)

Phys. Med. Biol. **58** (2013) 3283–3300 doi:10.1088/0031-9155/58/10/3283

Constrained reconstructions for 4D intervention guidance

J Kuntz[1,2], **B Flach**[1,2], **R Kueres**[1], **W Semmler**[1], **M Kachelrieß**[1,2] **and S Bartling**[1,3]

[1] German Cancer Research Center (DKFZ), Im Neuenheimer Feld 280, D-69120 Heidelberg, Germany
[2] Institute of Medical Physics, Friedrich-Alexander-University (FAU) Erlangen-Nürnberg, Henkestr 91, D-91052 Erlangen, Germany
[3] Institute of Clinical Radiology and Nuclear Medicine, University Medical Center Mannheim, Heidelberg University, Mannheim, Germany

E-mail: j.kuntz@dkfz.de

Received 27 December 2012, in final form 6 March 2013
Published 25 April 2013
Online at stacks.iop.org/PMB/58/3283

Abstract
Image-guided interventions are an increasingly important part of clinical minimally invasive procedures. However, up to now they cannot be performed under 4D (3D + time) guidance due to the exceedingly high x-ray dose. In this work we investigate the applicability of compressed sensing reconstructions for highly undersampled CT datasets combined with the incorporation of prior images in order to yield low dose 4D intervention guidance. We present a new reconstruction scheme *prior image dynamic interventional CT* (PrIDICT) that accounts for specific image features in intervention guidance and compare it to PICCS and ASD-POCS. The optimal parameters for the dose per projection and the numbers of projections per reconstruction are determined in phantom simulations and measurements. *In vivo* experiments in six pigs are performed in a cone-beam CT; measured doses are compared to current gold-standard intervention guidance represented by a clinical fluoroscopy system. Phantom studies show maximum image quality for identical overall doses in the range of 14 to 21 projections per reconstruction. *In vivo* studies reveal that interventional materials can be followed in 4D visualization and that PrIDICT, compared to PICCS and ASD-POCS, shows superior reconstruction results and fewer artifacts in the periphery with dose in the order of biplane fluoroscopy. These results suggest that 4D intervention guidance can be realized with today's flat detector and gantry systems using the herein presented reconstruction scheme.

(Some figures may appear in colour only in the online journal)

1. Introduction

Image-guided interventions are a growing field as they are often less-invasive, faster and more economic than comparable fully-invasive, surgical procedures. Here, interventional tools like

catheters and guide wires as well as vascular implants like stents and coils can be tracked within the body without direct line-of-sight. Continuous improvements in imaging hardware, e.g. high resolution flat detectors, have given rise to the development of more complex and more challenging procedures, allowing intravascular treatment of even more complex conditions (Cowen *et al* 2008). However, over the last decades the fundamental principle of interventional imaging remained unchanged. Intervention guidance is currently being performed using single- or biplane projective fluoroscopy. Due to the projective nature the interventionalist is left with uncertainties regarding the exact spatial position of interventional materials, which is especially disturbing in cases of complex procedures. Currently, the only means of gaining a three-dimensional (3D) understanding of the situation is by performing 3D data acquisition using slow rotation modes (5 to 20 s) of the C-arm (Cheung *et al* 2011, Prell *et al* 2010, Pfaff *et al* 2012). Computed tomography (CT) reconstructions of these datasets, which are typically acquired over an angular range of 180 to 240°, can be displayed in a fully 3D volume rendering of the scanned object. The orientation of the volume can be registered with position and orientation of the C-arm system and a fusion of the three-dimensional dataset together with fluoroscopy data is possible (Kroeze *et al* 2012). However, the 3D dataset becomes quickly outdated during the ongoing progress of the procedure.

Up to now, four-dimensional (4D) image guidance failed to reach its application in clinical practice, mainly due to high dose which is required for a continuous CT data acquisition using fully sampled datasets. However, during the course of an intervention most of the structures like bones and soft tissue remain unchanged. Only structures that are directly affected by the interventional process are changed. This fact especially becomes apparent in the case of neuroradiology interventions where only a miniscule volume (e.g. an aneurysm) may change between scans. Repetitive CT data acquisition therefore results in a large amount of redundancy in the raw datasets. If the amount of redundant data is reduced, the radiation dose exposure of patients and interventionalists can be reduced accordingly. One option to achieve this is the acquisition of highly undersampled datasets with only few projections. The reconstruction of these highly undersampled datasets with conventional algorithms would lead to prominent streak artifacts in the cross-sections. However, advanced algorithms using compressed sensing (CS) can deal with these data.

4D intervention guidance may be performed using CS-based algorithms as described in the following: a tomographic dataset showing the full anatomy without any interventional material or contrast agent, in the following called prior image, is acquired at the beginning of the procedure with full dose and a large number of projections. Followed by a contrast-enhanced scan with only a small number of projections and at low dose, that allows to reconstruct the vasculature as a 3D roadmap. All datasets for actual intervention guidance, in the following called time frames, can then be acquired with an extremely low number of projections, sufficient to reconstruct the changes induced by interventional materials and implants. For visualization, all three reconstructions can be combined and superimposed, showing the full anatomy, vasculature and the current setting of the interventional process, respectively. A general illustration showing the workflow in 4D intervention guidance is given in figure 1.

As standard CT reconstructions like the Feldkamp (FDK) algorithm (Feldkamp *et al* 1984) cannot incorporate additional information such as prior images or the information about specific image characteristics, the data acquisition in this case has to be performed with respect to the Shannon–Nyquist theorem with a large number of projections distributed over an angular range of at least (180° + fan angle) (Kak and Slaney 1988). First algorithms dealing with undersampled datasets and thus improving CT image quality by incorporating prior knowledge have been published more than two decades ago (McKinnon and Bates 1981),

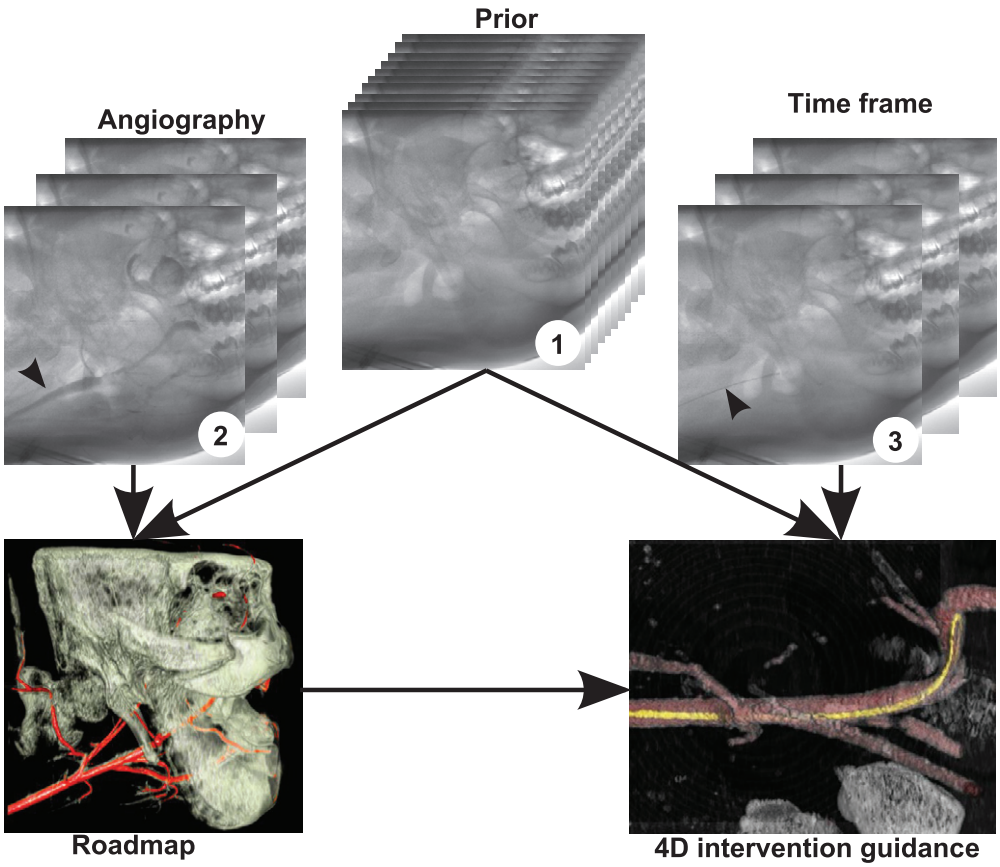

Figure 1. Illustrating the process of 4D intervention guidance with the three raw data acquisition steps. The prior image is acquired with a large number of projections, a contrast-enhanced angiography is acquired with high undersampling and the particular time frames for 4D intervention guidance are acquired with a high undersampling and low dose setting. The reconstruction of the interventional process can be displayed overlain with a roadmap, calculated based on the 3D angiographic reconstruction. Arrow tips point on contrast-enhanced vessels and a guidewire, respectively.

but the introduction of the CS theory by Candés *et al* (2006) and Donoho (2006) dramatically advanced the development of algorithms for undersampled reconstructions. This theory was originally described for a randomly sampled acquisition of Fourier coefficients in k-space. However, using this theory, magnetic resonance image reconstruction of pseudo-randomly sampled data (Lustig *et al* 2007) as well as CT reconstructions of highly undersampled raw data (Sidky and Pan 2008, Chen *et al* 2008b, Ritschl *et al* 2011) showed high accuracy, even if random sampling of raw data cannot be performed in CT data acquisition. While conventional iterative CT reconstruction algorithms usually aim at minimizing the l_2-norm

$$\min ||\mathsf{X}f - p||_2^2 \tag{1}$$

with the x-ray transform X, the image vector f and the measured raw data p, CS reconstructions aim at constraining this set of solutions. Only for fully sampled datasets, minimization of the l_2-norm leads to a unique solution, in case of undersampled raw data the result of e.g. algebraic reconstruction technique depends on the starting image f^0. As long as there is a transform

Ψ into a domain, in which the image is represented sparsely, CS can be used to formulate a constrained optimization

$$\min ||\Psi(f)||_1 \quad \text{subject to} \quad \min ||\mathsf{X}f - p||_2^2 \leqslant \epsilon. \tag{2}$$

Minimizing the l_1-norm of the sparsified image can be used to incorporate prior knowledge into the reconstructed image using the sparsifying transform Ψ while the raw data error does not exceed ϵ. Common sparsifying transforms are based e.g. on wavelets or the total variation (TV) (Chen *et al* 2008a, Sidky and Pan 2008, Sidky *et al* 2009). Using the TV minimization implies that, as prior information, the gradient of the reconstructed image has to be small. The minimization of the l_1-norm thereby is a surrogate for a minimization of l_0, which is computational complex and cannot be handled analytically. A direct inversion of the sparsifying transform usually is not necessary due to the iterative minimization process. Candés *et al* (2006) have shown that the number of independent measurements to reconstruct a slice image with the size of $N \times N$ and S significant pixels can be reconstructed using only $S \ln N$ independent and randomly distributed measurements. Several CT and tomosynthesis reconstruction algorithms using CS were published, mainly for specific tasks such as breast tomosynthesis (Sidky *et al* 2009), cardiac perfusion CT (Tang *et al* 2010, Park *et al* 2012) or angiography (Langet *et al* 2011). Even though interventional radiology being a repetitive scanning procedure with only few changes in the target area, and thus sparse difference images, is well-suited for CS reconstructions, up to now no specific reconstruction algorithm was published for 4D intervention guidance.

In this paper we introduce the concept of 4D intervention guidance using highly undersampled tomographic raw datasets and aim to investigate the usability of CS reconstructions for 4D intervention guidance. Here, we present a newly developed reconstruction algorithm called *prior image dynamic interventional computed tomography* (PrIDICT) that takes the specifics of intervention guidance into account, namely:

- existence of a high quality prior image without interventional materials
- differences of time frames and prior images are sparse
- imaging of high contrast structures is of the foremost interest in 4D intervention guidance
- tolerance to certain types of artifacts, especially to those that are not constant over time.

The PrIDICT algorithm is compared to the published algorithms *prior image constrained compressed sensing* (PICCS) (Chen *et al* 2008a) and a modified version of *adaptive steepest descent-projection onto convex sets* (ASD-POCS) (Sidky *et al* 2009). Optimal reconstruction parameters are analyzed in simulation and phantom measurements. This enables a direct comparison of the reconstruction algorithms. Additionally, these measurements allow finding the optimal number of projections on which a given overall dose is distributed so that an optimum in image quality is reached. Finally, the results of the phantom experiments are verified by examination of six pigs *in vivo* in a flat detector cone-beam CT (CBCT) system. Dose values of biplane fluoroscopy and the proposed 4D intervention guidance process are compared based on measurements in a clinical C-arm system and the gantry-based CBCT to investigate if dose in 4D intervention guidance is generally applicable for daily routine.

2. Material and methods

2.1. Algorithm design

2.1.1. Prior image constrained compressed sensing. PICCS uses the CS framework by restricting the set of solutions with a sparsifying function Ψ and a direct incorporation of a prior image, e.g. an image reconstructed with FDK using all raw data available. Starting

from that prior image, the correction of the image is performed iteratively by alternating the minimization of the raw data error with simultaneous algebraic reconstruction technique (SART) and a minimization step of the l_1 norm. The difference image of the current image f^n and the prior image f_p is calculated. Sparsifying and minimization are applied to both, the difference image $(f^n - f_p)$ as well as to the current image f^n. Both sparsifying transforms can but do not have to be equal. In analogy to Chen *et al* (2008a) we used the TV in both cases. Thus the minimization equation is

$$\min(\alpha||\mathrm{TV}(f - f_p)||_1 + (1-\alpha)||\mathrm{TV}(f)||_1) \text{ subject to } ||\mathsf{X}f - p||_2^2 \leqslant \epsilon \tag{3}$$

with p denoting the projections of the time frame and the weighting factor $\alpha \in [0, 1]$ controls the relative regularization impact to the difference image and the current image, respectively. Assuming the prior image, acquired with a large number of projections and a relatively high dose does not suffer from artifacts, in this paper the weighting was chosen empirically with $\alpha = 0.98$. Minimization was implemented as gradient descent with a fixed step length determined by prior experiments. The reconstruction process was terminated with a TV minimization step after a fixed number of 100 iterations.

2.1.2. Adaptive steepest descent-projection onto convex sets. ASD-POCS does not directly incorporate a prior image into the reconstruction but restricts only the current image with a TV sparsifying transform resulting in

$$\min ||\mathrm{TV}(f)||_1 \text{ subject to } ||\mathsf{X}f - p||_2^2 \leqslant \epsilon. \tag{4}$$

The ASD-POCS minimization equation thus is equal to the PICCS minimization when setting $\alpha = 0$. The key idea of ASD-POCS is to restrict the step length of both alternating steps raw data fidelity and TV minimization in each iteration, to assure convergence to the optimum solution. The ASD-POCS reconstruction was implemented according to the pseudo-code in Sidky *et al* (2009). According to the special settings in interventional radiology and the fact that we can incorporate a high quality prior image, we modified the ASD-POCS reconstruction to not constrain the current image but the difference image $(f - f_p)$ with the difference projection $(p - p_p)$, similar to the PICCS equation with $\alpha = 1$ the resulting minimization is

$$\min ||\mathrm{TV}(f - f_p)||_1 \text{ subject to } ||\mathsf{X}(f - f_p) - (p - p_p)||_2^2 \leqslant \epsilon'. \tag{5}$$

For ASD-POCS reconstructions, a total number of 100 iterations were performed.

2.1.3. Prior image dynamic interventional computed tomography. To comply with the special characteristics of intervention guidance approach combining undersampled time frames with high quality prior datasets, we developed a reconstruction algorithm called PrIDICT. This algorithm takes into account that difference images are ad hoc sparse in image domain and do not necessarily require additional sparsifying transforms. The main focus during intervention guidance is to monitor the high contrast changes provided by intervention instruments such as stents or guide wires in relation to the surrounding anatomy. This is the reason, why the difference images of the prior image f_p and the time frame f_t were reconstructed separately and added to the prior image afterwards. In particular, the PrIDICT reconstruction works as follows: a prior image f_p is reconstructed with a large number of projections using standard FDK reconstruction. The difference projection of the forward projection of the prior image and the measured raw data p of the time frames is calculated and reconstructed separately with a smooth reconstruction kernel (indicated by FDK_S); in our case we used the 1D convolution of a standard Ram–Lak kernel with a Gauß kernel.

$$f_u = \mathrm{FDK}_S(\mathsf{X}f^n - p). \tag{6}$$

To ensure a reduction of the raw data error, the update image is multiplied with a factor λ that minimizes the error to the raw data of the time frame

$$||\mathsf{X}(f^n + \lambda f_u) - p||_2^2. \tag{7}$$

From Candés *et al* (2006) it is known that at most $S = M/\ln N$ pixels of a $N \times N$ matrix can be reconstructed if M individual, independent measurements were sampled randomly. In the following this claim will be called the CS criterion. PrIDICT was designed to find an estimate for this CS criterion and reconstruct 4D datasets at a low dose using a heuristic approach that is not necessarily mathematically exact. Therefore, the sparsifying function Ψ in PrIDICT is defined preserving only the $M/\ln N$ pixels with the highest absolute value in the update image f_u, all other pixels are set to zero. Thus the actual image is described as

$$f^{n+1} = f^n + \lambda \Psi(f_u). \tag{8}$$

This process is performed iteratively while the update image is added to the current image after every iteration step. In the current implementation we used a fixed number of ten iterations as these result in sufficient image quality analyzed in pilot tests.

2.2. Analysis of the CS reconstructions for intervention guidance

The challenge in 4D intervention guidance is to reconstruct reliable image sequences while maintaining x-ray doses as low as possible. In CT imaging, a given overall x-ray dose can be distributed on rather few projections with a relatively high dose per projection, or many projections with a relative low x-ray dose per projection. In standard CT reconstruction the latter is preferred, because a larger amount of projections prevents undersampling artifacts, while CS reconstructions can compensate for these artifacts. Therefore, quality analyses were performed for reconstruction series with various numbers of projections and constant dose to identify optimal raw data acquisition parameters.

2.2.1. Simulations and phantom studies. Quality analyses were performed using both, mathematical phantom simulations and real phantom measurements. The aim was to investigate whether optimum scanning parameters exist and which number of projections results in the maximum image quality if the overall dose is kept constant. Simulations were performed with a simple stent phantom showing linear struts inserted into a water-equivalent cylinder. A same-sized phantom was manufactured and investigated in a CBCT with a real stent inserted into a water-filled bore representing a blood vessel. Geometry and trajectory of the data acquisition were identical in simulations and real phantom measurements, respectively. Full-sampled datasets (630 projections) without stent were used in both cases to perform a reconstruction of the prior image without additional noise. Highly undersampled datasets (9–76 overall projections), showing the stent inserted into the bore were used to reconstruct the time frames. The overall dose for the time frames was kept virtually constant by adding an appropriate amount of Gaussian-distributed noise to the projection images, thereby three dose levels were used in the simulation study (210k, 420k and 840k photons) and for the real phantom measurements (21k, 42k and 84k photons). Note the factor ten reduced dose for real phantom measurements all the while the struts show higher densities. No additional constant noise offset representing e.g. electronic noise was simulated in the projection images.

Simulated phantom. A water-equivalent cylinder with a diameter of 60 mm and a bore size of 6 mm, inclined by 10° to the z-axis was simulated. The stent simulation was built using eight cylindrical struts with a diameter of 0.7 mm and a contrast of 1000 HU to the surrounding material.

Real phantom. The real phantom was built of polymethylmethacrylate with a diameter of 60 mm showing about 60 HU in the CBCT scans. A centered bore with 8 mm was filled with water. For time frame scans a stent (Boston Scientific, Wallstent-Uni, length 40 mm, strut diameter 0.185 mm) was inserted into the bore, maximum CT numbers in the wall stent were up to 8000 HU.

2.2.2. Analysis of image quality. Image quality was investigated by visual inspection of cross-sections as well as quantitatively using the Pearson correlation (PC) and the mean squared contingency (MSC) of a binary segmented image. To maximize the effect in image quality analyses, all static structures in the prior image were removed and only differences to the prior, called update images f_u, were compared. Undersampled update reconstructions were compared to fully sampled reference updates $f_{u\,\mathrm{Ref}}$ reconstructed with FDK without the addition of image noise. Also for the simulations the FDK reconstruction was used instead of the true image to preserve consistency to real phantom measurements, where no true image is available and the FDK reconstruction of the fully sampled dataset acts as a surrogate ground truth.

Pearson correlation. The PC is a measure of the degree of linear correlation of the two image vectors $f_{u\,\mathrm{Ref}}$ and f_u with a total dynamic range of $[-1, 1]$. It is defined as

$$\mathrm{PC}(f_{u\,\mathrm{Ref}}, f_u) = \frac{\mathrm{COV}(f_{u\,\mathrm{Ref}}, f_u)}{\sigma(f_{u\,\mathrm{Ref}})\sigma(f_u)} \tag{9}$$

where COV is the covariance and σ is the standard deviation. As PC does not take the absolute CT values into account but only the linear correlation, it can describe the detectability of the stent inserts and structures and does not assess the absolute correctness of the CT values.

Mean squared contingency. To analyze the possibility of detecting structures with homogeneous CT values, we also calculated the MSC of a binary segmented image using a cross tabulation. For the segmentation dynamic thresholds from 5% to 95% of the stent contrast were calculated and the highest accordance with the analogously segmented reference was used as MSC. Using the binary segmentation, this approach ignores artifacts with lower contrast, similar to an optimized windowing, where some artifacts might be invisible and do not affect the intervention guidance. Thus this parameter gives an adequate degree of the maximum possible detectability of structures using ideal windowing, even if this is not applicable in real world applications where no reference images are available.

2.2.3. Animal experiments. All animal experiments performed in this study were approved by the governmental animal ethics committee (Regierungspräsidium Karlsruhe). Several interventional processes were performed in six pig models (35 to 65 kg, three to six months old). Anesthetized animals (1 mg kg^{-1} Midazolam, 20 mg kg^{-1} Ketamin, 8 mg kg^{-1} Azaperon) were positioned head first in the iso-center of the gantry. A high resolution prior scan was performed with 19 s per rotation without any contrast agent injected or interventional material inserted into the vessels. Afterwards, contrasted scans were performed with a rotation speed of 5 s while contrast agent (Imeron 300, Bracco Diagnostic Imaging Group, Princeton, USA) was injected with a flow rate of 2 ml s^{-1} to image the vascular tree and a roadmap was calculated. In the following interventional processes, vessel probing was performed with guide wires (e.g. Boston Scientific Starter, diameter 0.035 inch) and catheters (e.g. Radiofocus angiography catheter vertebral, Terumo). Stents were placed into the animal's carotid artery and expanded during continuous raw data acquisition. During all interventional tasks, raw data acquisition was performed in a CBCT. The CBCT system was based on a clinical CT gantry with a flat detector providing a maximum field of view (FOV) of 240 $\times$ 180 mm^2 in the iso-center and a

spatial resolution of approximately 200 μm (Gupta *et al* 2006). Acquisition parameters were 4 s/rot and 120 projections (1024 $\times$ 768 pixels, 2 $\times$ 2 binning mode) per rotation. Image reconstruction for animal experiments was performed with 630 projections distributed over approximately 395° using FDK for the prior image. Angiography datasets were reconstructed using the PICCS reconstruction algorithm in an undersampled setting with 16 projections distributed over 180° without additional noise added to the projections. Time frames of the interventional procedures were reconstructed also with 16 projections per reconstruction, equally distributed over 180° with three dose levels using all three reconstructions PICCS, ASD-POCS and PrIDICT.

2.2.4. Dose measurements. Due to the fundamental different imaging characteristics and dose distributions of projective and tomographic imaging, dose comparison of 2D and 3D modalities in general is a challenging task. Several approaches for dose measurements in CBCT systems were proposed (Fahrig *et al* 2006, Gupta *et al* 2006) but no standardized measurements for intermodality comparison are available. Furthermore, an automated exposure control is used in interventional C-arm systems and therefore, the dose exposure depends on the object geometry and size. In the used CBCT, no exposure control is implemented and imaging parameters are selected manually. For direct comparison of 4D intervention guidance with the dose required in a clinical biplane fluoroscopy system, a customized measurement technique was used in this work. We employed a large CTDI phantom (diameter 160 mm, length 320 mm), where we measured the air kerma with a pencil beam ionization chamber (PTW Freiburg, Type 30009) in the centered bore at various positions and integrated over the z-axis acted as an internal reference in this comparison. The herein measured dose must not be compared to published surrogate markers such as effective dose. The automated exposure control induces a constant dose at the detector so the CTDI phantom leads to a realistic dose profile. The FOV in both modalities was chosen identically with 240 $\times$ 180 mm^2 in the iso-center. The setup was irradiated from various directions in the fluoroscopy system with 7.5 fps, 72 kV pulsed (parameters displayed for the last acquired projection) and over one full rotation in the CBCT system with 30 fps, 80 kV and 50 mA pulsed (effective tube current approx. 18 mA).

3. Results

The results are divided into two sections. In the first section the simulations and phantom measurements are shown as representative images and quality analyses respectively. The optimal acquisition parameters indicated in the first section were used for the proof of concept study. In the second part, cross-sections and volume renderings of actually performed interventional procedures in pigs are displayed. Applied dose was compared to those of conventional biplane fluoroscopy.

3.1. Simulations and phantom measurements

As reference, all available projections of the time frame, distributed over an angular range of 360° were reconstructed using a standard FDK algorithm. This reference was used for visual comparison to the undersampled reconstructions as well as for automated quality analyses. Cross-sections of the simulation and phantom studies are shown in figure 2, reconstructed with standard FDK. The prior image as well as the reconstruction of the fully sampled time frame was based on 630 projections, for the undersampled time frame in figure 2 a reduced dataset with 17 projections was used.

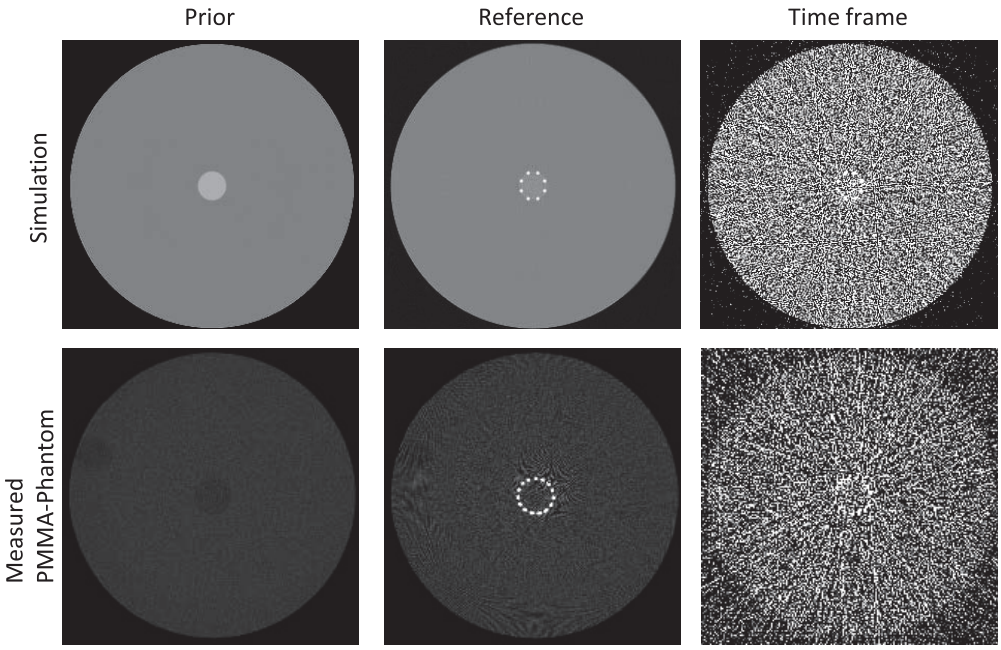

Figure 2. Standard reconstructions of the prior image, the fully sampled reference and the undersampled time frame using 17 projections for simulations and phantom measurements. Prior images were directly incorporated into the CS reconstructions. Reference images are provided for comparison with undersampled reconstructions in consecutive figures. The undersampled standard reconstructions of the time frame result in strong artifacts inhibiting usage for intervention guidance.

Undersampled time frames were reconstructed with both, the FDK and SART reconstructions for comparison. While the prior image cannot be incorporated into the FDK reconstruction, it was used as start image f^0 in the SART reconstruction. The cross-sections reconstructed with FDK were dominated by streak artifacts and a very high noise level. Neither the contrasted inner bore nor the stents struts were clearly visible (figure 2, time frame). Reconstructions with SART shown in figure 3 were dominated by high noise levels as well, but stent struts are visible.

Image reconstruction results in dependence of the number of projections are shown in figure 4 of all three reconstruction algorithms (PICCS, ASD-POCS and PrIDICT) for mathematical simulations and phantom measurements, respectively. Compared to the reconstructions with SART using identical prior and time frame datasets, the CS reconstructions showed a much lower noise level. Only in the PICCS reconstruction of the simulation using nine projections the stent was not visible. In all other reconstructions the stent was clearly visible and the struts were depicted clearly and separable in reconstructions using 11 to 17 projections. In this range, visual inspection showed the best image quality. The resulting noise in reconstructions using PICCS and PrIDICT increased with higher numbers of projections, while the ASD-POCS reconstruction retained nearly constant noise levels over the whole range. PICCS showed laminar, low frequency artifacts for a wide range of projections and resulted in higher frequency noise in the reconstructions using 42 projections. ASD-POCS and PrIDICT did not show these laminar artifacts, instead they were affected by speckle noise and especially in PrIDICT artifacts increased using higher numbers of projections. Compared to the reference images in figure 2, PICCS reconstructed struts with

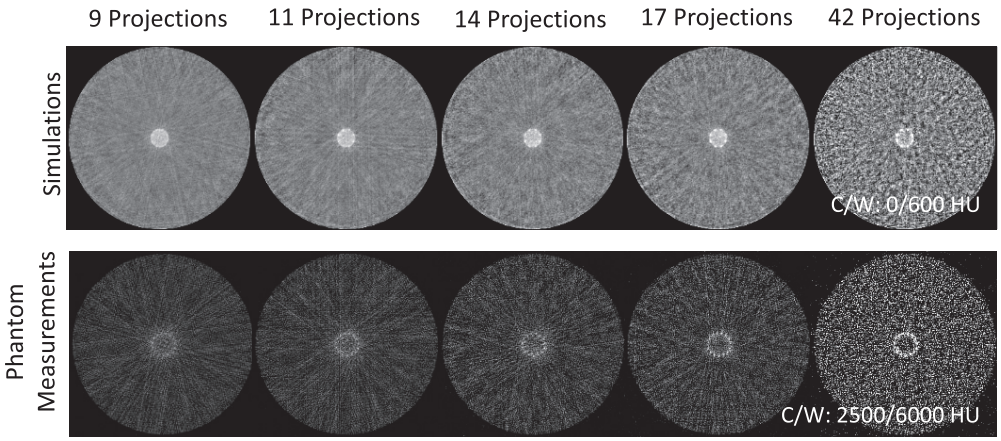

Figure 3. Cross-sections of the stent phantom simulations and real phantom measurements reconstructed with 9 to 42 projections from time frames using SART reconstruction. As start image for the SART the prior image, reconstructed with FDK was used. Both reconstruction series hardly show the stent struts, and resulting images are dominated by noise and undersampling artifacts.

realistic diameters, while they were represented too small and deformed in ASD-POCS and dilated and slightly blurred in PrIDICT.

Quantitative image analyses in general followed the results of the visual inspections. Figure 5 shows the MSC and the PC correlation for the three reconstruction algorithms as a function of the number of projections. In concordance with the visual inspection, the maximum image quality using PICCS was in the range of 14 to 21 projections for both quality parameters in simulations and real phantom measurements. Maximum image quality slightly shifted to more projections using higher overall dose levels. The ASD-POCS reconstructions showed a nearly constant image quality consistent for both comparison parameters, which was in line with the visual inspections. The maximum image qualities were slightly lower than those for PICCS reconstructions. The PrIDICT reconstruction quality analyses again showed maximum image quality in the area of 14 to 21 projections for both PC and MSC parameters. While the PC was completely conform to the visual inspection over the whole range and showed minimum values for the largest number of projections, the MSC showed an increase for the 76 projections point in the binary segmentation of the PrIDICT reconstructions, what was not conform to the visual inspection of the cross-sections.

3.2. Animal experiments

The undersampled time frame reconstructions of *in vivo* animal studies resulted in 4D datasets where the interventional materials were clearly visible in all reconstructed phases. Position and orientation of the interventional material was clearly depicted with respect to the surrounding structures and the vasculature. The reconstructed time frames could be displayed with angiographic roadmaps overlain. The following examples are provided: one time frame showing the expansion of a stent in the carotid artery is shown in figure 6, reconstructed with PICCS, ASD-POCS and PrIDICT, respectively where a prior image of 630 projections was combined with 16 projections of the time frame. For a direct comparison of the image quality of all three algorithms, the same phase was reconstructed with three different dose levels (*undersampled dose, low-dose, ultra low-dose*, see table 1) using 16 projections each. For

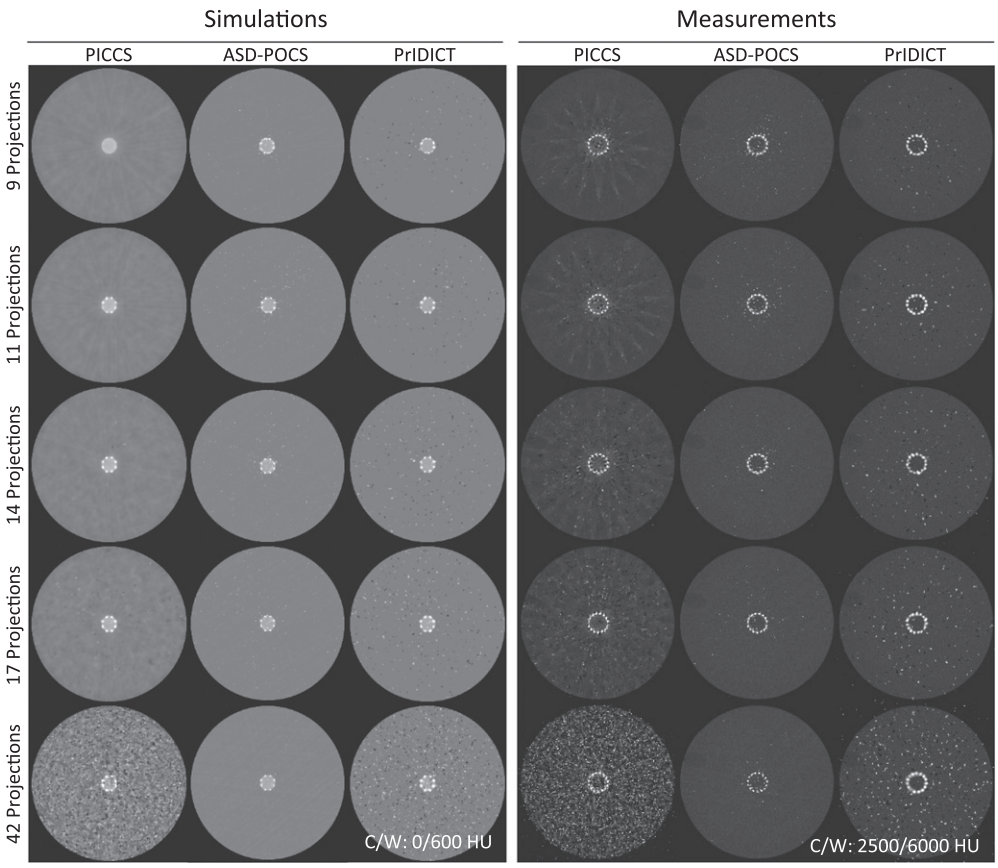

Figure 4. Undersampled time frames, reconstructed with PICCS, ASD-POCS and PrIDICT incorporating prior images are shown. All simulations were reconstructed with an overall dose of 210k photons per time frame, distributed over 9 to 42 projections. Best visual image quality can be observed using 11 to 17 projections. Both, more and less projections are afflicted with undersampling artifacts or higher noise levels. ASD-POCS shows the highest constancy over a wide range of total projections.

Table 1. Dose comparison of single plane 2D fluoroscopy in a standard clinical device and newly developed 4D intervention guidance in the experimental implementation in a CBCT system. Acquisition parameters for both modalities are provided. Furthermore actual dose levels as well as dose levels for simulated *undersampled* acquisition, *low-dose* and *ultra low-dose* are given. Comparing to biplane fluoroscopy with the doubled dose, 4D intervention guidance can be performed with an even lower dose using the *ultra low-dose* setting.

		4D intervention guidance			
	Artis zee	Prior-image	Under sampled	Low-dose	Ultra-low dose
Tube voltage (kV)	60	80	80	80	80
Tube current (mA)	2	18	9.6	1.92	0.44
Acquisition time (s)	1	21	1	1	1
Chamber current (pA)	2.26	117.4	59.6	11.9	2.7
Air-kerma-length-product (μGy cm)	186	192 701	4894	978.8	222.5
Air-kerma (μGy)	10.3	10 706	271.9	54.4	12.4

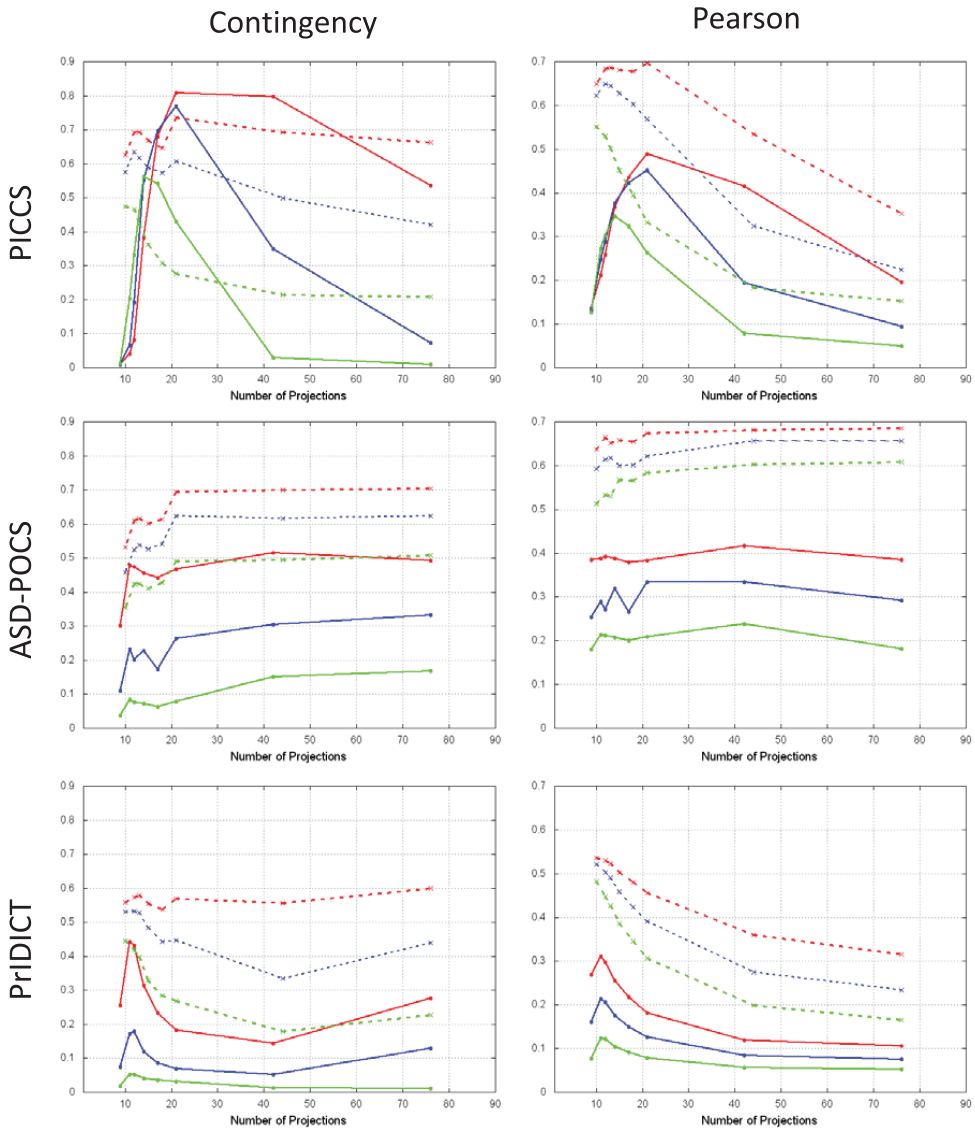

Figure 5. Quantitative image quality analyses are plotted over the number of projections while in every series the overall dose was kept constant. Solid lines show the simulation results of the stent phantom at 210k photons (green), 420k photons (blue) and 840k photons (red). Dotted plots show the results in real phantom measurements with 21k, 42k and 84k photons, respectively. Maximum image quality in PICCS and PrIDICT is clearly located in the area of 11 to 17 projections. ASD-POCS shows nearly constant image quality.

low-dose and *ultra low-dose* reconstructions, dose was virtually reduced by adding additional noise to the projection images. To assess the impact of the artifacts and relevant image features, difference images of the time frame and the prior image were calculated. While reconstructions with *undersampled dose* provided nearly identical representations of the stent, the artifacts increased in the *low-dose* reconstructions. Here, PICCS also showed laminar artifacts in the surrounding tissue and some salt and pepper noise texture. ASD-POCS and PrIDICT showed nearly same noise levels without laminar artifacts in the difference images.

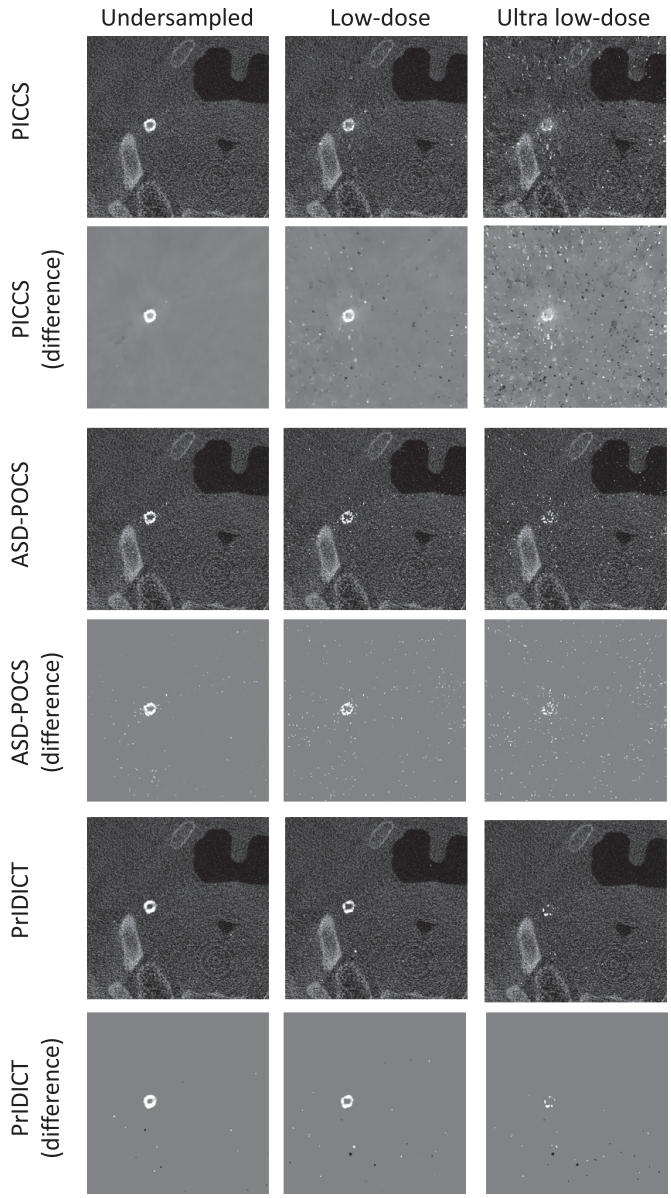

Figure 6. Cross-sections of one time frame during the stenting of the common carotid artery in a pig. Three dose levels are shown, reconstructed with PICCS, ASD-POCS and PrIDICT (C/W 500/2000 HU). The fully sampled prior image was acquired without interventional materials while the only difference to the undersampled time frame is the insertion of the stent. Difference images of the reconstructed time frame and the prior image show the stent and image artifacts (C/W 0/2000 HU). While artifacts in PICCS and ASD-POCS are distributed over the whole image, PrIDICT artifacts are embodied in single spots with relatively high intensities.

Stent representations were very similar in all *low-dose* reconstructions; visually no relevant loss of information could be recognized. The *ultra low-dose* reconstructions clearly showed increasing noise in the difference image as well as in the direct time frame reconstructions. Noise in the peripheries had the highest impact in the PICCS reconstructions, while ASD-POCS

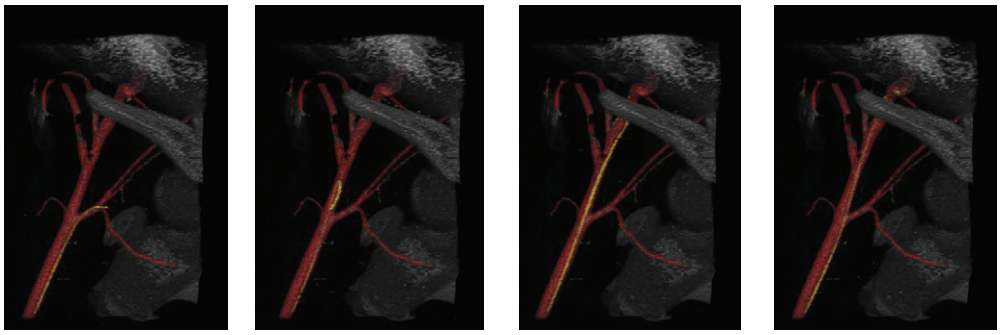

Figure 7. Volume renderings of four exemplary time frames reconstructed with a prior dataset of 630 projections, 16 projections of an angiography dataset were used to calculate a roadmap (red) with PICCS and again 16 projections with simulated *low-dose* were used to reconstruct the guidewire (yellow) time frames with PrIDICT. Position and orientation of the guide wire tip is clearly depicted in every single time frame reconstruction.

and PrIDICT showed less noise but also an explicitly lower accuracy of the stent representation. However, this effect changed in z-direction and had a minor role for 4D intervention guidance. Additional video material of the 4D volume rendering of the stent expansion is available at 4D-CATH.dkfz.de.

Time frames of a guide wire probing in the common carotid artery reconstructed with PrIDICT are shown in figure 7, where the vasculature, highlighted as roadmap, was reconstructed with PICCS. Every single time frame shows a period of 2 s; in this figure only four reconstructions with an intermediate period of 4 s are shown. A video of the full time series can be accessed at 4D-CATH.dkfz.de. In these 4D datasets, parts of the anatomy, blocking the view to subjacent structures, were virtually removed in the volume rendering.

3.3. Dose comparison

Dose values were measured for a single plane setting. To compare to biplane fluoroscopy mode we used the doubled dose. The measured doses (air kerma) in the pencil ionization chamber and the corresponding tube parameters are listed in table 1. Compared to the dose of biplane fluoroscopy (20.6 μGy s^{-1}) the dose of 4D intervention guidance with fully sampled CBCT datasets was more than 1000-fold. Such 4D imaging would thus result in an unacceptable high dose. Using undersampled datasets, the dose could be lowered to the 13-fold of biplane fluoroscopy. At this dose level the initial road maps were acquired. In the *low-dose* setting with only the doubled dose of biplane fluoroscopy, minor artifacts were visible in the reconstructions. Image quality was still sufficient for 4D intervention guidance. Even in the *ultra low-dose* setting with doses below the biplane fluoroscopy dose level, resulting image information was still sufficient to guide an intervention in a 4D setting.

4. Discussion

Reconstruction for 4D intervention guidance aims at achieving sufficient image quality while patient dose is reduced to a minimum. It was shown in simulations and phantom studies that this can be reached with few (14 to 21) projections. In literature it was shown that sufficient image quality can be achieved with the same low amount of projections when dealing with similar reconstruction problems, e.g. cardiac imaging (Chen *et al* 2012)

(16 to 17 projections), angiography (Han *et al* 2012) (3 to 9 noise-free projections) and in kyphoplasty (Lee *et al* 2012) (15 projections). Unlike conventional reconstruction algorithms (e.g. FDK or SART), CS reconstructions can deal with the undersampled raw data and suppress streak artifacts. Increasing the number of projections with a constant dose per reconstruction resulted in higher noise in the reconstructed images. Trying to compensate this by providing more strength to the regularization term would lead to a suppression of the sparse image features of the interventional material. All phantom studies were performed without simulating electronic noise. Therefore the decrease in image quality for larger numbers of projections would be even higher for real world applications, unless photon counting detectors are available in clinical systems.

PICCS and ASD-POCS use alternating optimization of the raw data error and the reduction of the TV with a gradient descent optimization. Comparing the forward projection of a high quality prior image and a low dose time frame projection, main differences arise from noise and usually not from the inserted interventional material. Consequently applying TV minimization to these datasets would lead to the suppression of not only noise but also the interventional materials in reconstructions, while mainly laminar artifacts would be reconstructed instead (compare figure 4, PICCS reconstruction with nine projections). In contrast, PrIDICT tries to solve the reconstruction problem with a heuristic but efficient approach combining the FDK reconstruction with the constraint that only few pixels are containing the desired information. In contrast to the TV reconstructions, this enforces the reconstruction of few changes, while a sparse TV usually promotes laminar structures. So PrIDICT accounts for specific feature of minimally invasive interventional radiology.

In *in vivo* experiments the interventional material was visible in reconstructions with all three algorithms. However, there were large differences in image quality which provided insights in the relationship between image features and different constrains in the reconstruction algorithms. This will be discussed in the following. Roadmaps were reconstructed with undersampled dose using PICCS instead of PrIDICT as the number of significant pixels representing the vasculature is higher than the CS criterion in PrIDICT allowed while the TV minimization in PICCS assured a sufficient reconstruction of the contrasted vessels. In contrast to this, ultra low-dose reconstructions of time frames using PICCS resulted in laminar artifacts and therefore compromised the representation of the surrounding tissue and decreased the contrast of the stent. Here, PrIDICT showed its advantages in intervention guidance. Even though parts of the stent were missing in the cross-sections, these artifacts, as well as the salt and pepper-like noise, were neither constant over time nor over the z-position of the reconstruction. Therefore, interventionalists could easily distinguish them from inserted instruments. Concluding from this, PrIDICT showed its superiority for 4D intervention guidance over other, published CS-based algorithms.

Our data suggest that a dramatic dose reduction for 4D intervention guidance compared to repetitive standard CBCT scans is feasible without losing spatial information of the position of interventional materials. The direct dose comparison indicates that 4D intervention guidance can be realized with the same low dose as biplane fluoroscopy which serves as current gold-standard in intervention guidance. This comparison, however, is limited with respect to the following points.

- 4D intervention guidance dose was measured in a prototype CBCT, not optimized for this task (e.g. it had a different x-ray spectrum than the C-arm system and no automated exposure control).
- The CTDI phantom was smaller (diameter 160 mm) than the pig's head (diameter approximately 240 mm) which lead to a lower dose due to the automatic exposure control

in the C-arm system. *In vivo* measurements using the C-arm system would result in higher doses.

- The temporal resolution of both systems was different; however equal frame rates can be achieved using shifted reconstructions.

The dose used for the acquisition of the 3D roadmap, exceeding tenfold of the biplane fluoroscopy, is relatively high. However, one 3D roadmap can potentially replace multiple projective roadmaps as it can be displayed in any desired orientation and therefore reduce the overall dose in practice. 4D intervention guidance can provide more information than projective fluoroscopy, speeding up the overall intervention or enabling the introduction of novel minimally invasive interventions. A higher dose per time unit could become tolerable giving the advantages of the 4D intervention guidance. Further investigations in real-time interventions and clinical trials are needed in order to assess the required temporal resolution and the overall dose per intervention in 4D intervention guidance.

Time-resolved volume renderings, presented here, are displayed in manually selected orientation and optimized transfer functions. In future clinical systems this might be performed with automated algorithms that recommend specific orientations to the interventionalist and give an initial transfer function, which can be customized if necessary. The clinical implementation of 4D intervention guidance systems may necessitate development of useful, partially automated visualization methods.

While reconstructions of the prior image were performed with FDK, the time frames were reconstructed with computationally more demanding, iterative reconstructions. PICCS and ASD-POCS reconstructions were stopped after 100 overall iterations; PrIDICT was terminated after 10 iterations. The reconstruction code we used was not optimized for reconstruction speed, so calculation times from minutes up to several hours were required on a multi-core PC system (Fujitsu Celsius R670, 2 $\times$ Intel Xeon x5690, 96 GB RAM). However, due to the sparse sampling and the resulting few projection and backprojection steps, such calculations can be technically performed with minimal delay and in real-time. For example, a 512^3 voxel volume currently can be reconstructed with standard techniques from 496 projections (1248 $\times$ 960 pixels) in 3.4 s on an NVIDIA GTX 670 graphics device (Rohkohl *et al* 2009). The calculation for PrIDICT could be distributed to several devices to further speed it up since the reconstruction is ideally suited for parallelization.

Due to the limited rotation speed, the relatively low readout rates and lack of the possibility to acquire only few projections per 360° in this proof-of-concept setup all reconstructions were performed off-line with retrospective undersampling and low-dose simulations. Interventional materials were moved relatively slow to be able to perform time frame reconstructions from 180° and 2 s, respectively. Further analyses of the required temporal resolution for complex interventional procedures will be needed once dedicated clinical systems come into practice. Since modern gantries perform up to three rotations per second and flat detectors provide readout rates of 60 fps or more, the concept of 4D intervention guidance could be realized with sufficient temporal resolution. Although this work was performed with a continuously rotating flat detector CT system, parts of this work can be applied in current C-arm systems. The capability of real-time imaging will be lost in this case due to limited rotation speed and rotation range, however, a large dose reduction e.g. for biopsies, can be achieved.

5. Conclusion

In this proof of concept study it was shown that 4D intervention guidance is possible with today's flat detectors and gantry-based CT systems, while doses in the range of current

biplane fluoroscopy can be reached. The proposed reconstruction algorithm shows advantages specific to intervention guidance compared to other CS reconstruction algorithms. Using the approach demonstrated in this work, real-time 4D guidance can become clinically available, new intervention guidance processes might be achieved and help to minimize the invasiveness of image-guided interventions. They can make interventional radiology safer and faster with great benefit for patients' health.

Acknowledgments

The research is funded by the DFG (German Research Foundation) grant (KA 1678/6-1 and BA 3546/2-1). The high-speed image reconstruction software RayConStruct-IR was provided by RayConStruct®GmbH, Nürnberg, Germany. We thank Dr Michaela Socher and Roland Galmbacher for animal handling. We would like to thank Dr Andreas Maier and PD Dr Yiannis Kyriakou for extensive help with the experimental setup as well as discussion of applications, clinical implementation and future developments.

References

Candes E J, Romberg J and Tao T 2006 Robust uncertainty principles: exact signal reconstruction from highly incomplete frequency information *IEEE J. Inform. Technol.* **52** 489–509

Chen G-H, Tang J and Leng S 2008a Prior image constrained compressed sensing (PICCS) *Proc. SPIE* **6856** 685618

Chen G-H, Tang J and Leng S 2008b Prior image constrained compressed sensing (PICCS): a method to accurately reconstruct dynamic CT images from highly undersampled projection data sets *Med. Phys.* **35** 660–3

Chen G-H *et al* 2012 Time-resolved interventional cardiac C-arm cone-beam CT: an application of the PICCS algorithm *IEEE Trans. Med. Imaging* **31** 907–23

Cheung J Y, Kim Y, Shim S S and Lim S M 2011 Combined fluoroscopy- and CT-guided transthoracic needle biopsy using a C-arm cone-beam CT system: comparison with fluoroscopy-guided biopsy *Korean J. Radiol.* **12** 89–96

Cowen A R, Davies A G and Sivananthan M U 2008 The design and imaging characteristics of dynamic, solid-state, flat-panel x-ray image detectors for digital fluoroscopy and fluorography *Clin. Radiol.* **63** 1073–85

Donoho D L 2006 Compressed sensing *IEEE Trans. Inform. Theory* **52** 1289–306

Fahrig R, Dixon R, Payne T, Morin R L, Ganguly A and Strobel N 2006 Dose and image quality for a cone-beam C-arm CT system *Med. Phys.* **33** 4541–50

Feldkamp L A, Davis L C and Kress J W 1984 Practical cone-beam algorithm *J. Opt. Soc. Am.* **1** 612–9

Gupta R, Grasruck M, Suess C, Bartling S H, Schmidt B, Stierstorfer K, Popescu S, Brady T and Flohr T 2006 Ultra-high resolution flat-panel volume CT: fundamental principles, design architecture, and system characterization *Eur. Radiol.* **16** 1191–205

Han X, Bian J, Ritman E L, Sidky E Y and Pan X 2012 Optimization-based reconstruction of sparse images from few-view projections *Phys. Med. Biol.* **57** 5245–73

Kak A C and Slaney M 1988 *Principles of Computerized Tomographic Imaging* (New York: IEEE)

Kroeze S G C, Huisman M, Verkooijen H M, van Diest P J, Ruud Bosch J L H and van den Bosch M A A J 2012 Real-time 3D fluoroscopy-guided large core needle biopsy of renal masses: a critical early evaluation according to the ideal recommendations *Cardiovasc. Intervent. Radiol.* **35** 680–5

Langet H, Riddell C, Trousset Y, Tenenhaus A, Lahalle E, Fleury G and Paragios N 2011 Compressed sensing based 3D tomographic reconstruction for rotational angiography *MICCAI 2011: Proc. 14th Int. Conf. on Medical Image Computing and Computer-Assisted Intervention* vol 14 pp 97–104

Lee H, Xing L, Davidi R, Li R, Qian J and Lee R 2012 Improved compressed sensing-based cone-beam CT reconstruction using adaptive prior image constraints *Phys. Med. Biol.* **57** 2287–307

Lustig M, Donoho D and Pauly J M 2007 Sparse MRI: the application of compressed sensing for rapid MR imaging *Magn. Reson. Med.* **58** 1182–95

McKinnon G C and Bates R H 1981 Towards imaging the beating heart usefully with a conventional CT scanner *IEEE Trans. Biomed. Eng.* **28** 123–7

Park J C, Song B, Kim J S, Park S H, Kim H K, Liu Z, Suh T S and Song W Y 2012 Fast compressed sensing-based CBCT reconstruction using Barzilai–Borwein formulation for application to on-line IGRT *Med. Phys.* **39** 1207–17

Pfaff J, Struffert T, Gölitz P and Dörfler A 2012 Angiographic CT for intraprocedural monitoring of complex neuroendovascular procedures *Am. J. Neuroradiol.* (epub ahead of print, doi:10.3174/ajnr.A3014)

Prell D, Kyriakou Y, Struffert T, Dörfler A and Kalender W A 2010 Metal artifact reduction for clipping and coiling in interventional C-arm CT *Am. J. Neuroradiol.* **31** 634–9

Ritschl L, Bergner F, Fleischmann C and Kachelrieß M 2011 Improved total variation-based CT image reconstruction applied to clinical data *Phys. Med. Biol.* **56** 1545–61

Rohkohl C, Keck B, Hofmann H and Hornegger J 2009 RabbitCT—an open platform for benchmarking 3D cone-beam reconstruction algorithms *Med. Phys.* **36** 3940–4

Sidky E Y and Pan X 2008 Image reconstruction in circular cone-beam computed tomography by constrained, total-variation minimization *Phys. Med. Biol.* **53** 4777–807

Sidky E Y, Pan X, Reiser I S, Nishikawa R M, Moore R H and Kopans D B 2009 Enhanced imaging of microcalcifications in digital breast tomosynthesis through improved image-reconstruction algorithms *Med. Phys.* **36** 4920–32

Tang J, Hsieh J and Chen G-H 2010 Temporal resolution improvement in cardiac CT using PICCS (TRI-PICCS): performance studies *Med. Phys.* **37** 4377–88